6th European Advanced Accelerator Concepts Workshop IOP Publishing
Journal of Physics: Conference Series **3124** (2025) 012019 doi:10.1088/1742-6596/3124/1/012019

Characterization of Liquid Micro-Droplets for Laser-Driven Proton Acceleration

M. C. Nolte[1], G. A. Becker[1], M. Beyer[1,2], M. B. Schwab[1,2], M. Hornung[1,2], M. Hellwing[1] and M. C. Kaluza[1,2]

[1] Institute of Optics and Quantum Electronics, Jena, Germany
[2] Helmholtz Institute Jena, Jena, Germany

E-mail: `mathis.nolte@uni-jena.de`

Abstract. In laser-driven particle acceleration the choice of target material can have a huge impact on the acceleration process. Therefore, a laser-driven proton acceleration experiment was conducted at the POLARIS laser facility, in which liquid micro-droplets made of water or ethylene glycole were used as targets. Droplet chains were created by a pressurized capillary nozzle, which was made to vibrate with an oscillating piezo element. The driving frequency was synchronized to the laser pulses to create stable droplets for each laser shot. The stability of the droplets was examined for different pressures, driving frequencies and liquid types. The droplets were then irradiated by laser pulses from the POLARIS laser system, which had intensites up to $4 \times 10^{19}\,\mathrm{W\,cm^{-2}}$ and accelerated protons via the TNSA-mechanism. The shape of the resulting proton beam was observed with a scintillator, while its energy spectrum in the forward direction was simultaneously measured with a Thomson parabola. In the experiments, the proton beam profile from water droplets showed modulations in the beam intensity, which could be strongly reduced by using ethylene glycol. A possible explanation for these modulations could be the electric fields, which are created in the background gas. Since ethylene glycole has a much lower vapor pressure, the modulations are then less pronounced.

1. Introduction

Proton beams accelerated from a laser-generated plasma have various potential applications. Examples are proton therapy for cancer treatment [1] or fusion research [2]. The acceleration process depends on the specific parameters of the used laser pulse, but also the used target material and the target shape have a significant impact on it.

Frequently used targets are thin foils. However, the electric field driving the ion acceleration from the rear side can be weakened, if the electrons leave the interaction zone along the foil surface [3]. To avoid this problem, mass or volume limited-targets can be used, which have limited extensions in all three spatial dimensions. A way to obtain these targets is the generation of micro-droplets from liquid jets. A further advantage of this approach is the possibility to observe the laser-target interaction, e. g. with shadowgraphy, which is more complicated for targets such as laterally extended foils. To hit these droplets reliably with each laser pulse, however, the breakup process needs to be stable. Hence, in this work, the creation of micro droplets consisting of water and ethylene glycol is examined. Furthermore, the results from an acceleration experiment at the POLARIS laser system are presented.

Journal of Physics: Conference Series **3124** (2025) 012019 doi:10.1088/1742-6596/3124/1/012019

2. Creation of Liquid Micro-Doplets

To use micrometer-sized droplets as a target for laser-plasma experiments, they have to be hit reliably by each laser shot. Therefore, it is important to create a temporally and spatially stable droplet chain from a liquid jet. For that, the Rayleigh-Plateau instability can be exploited. A liquid jet, which has small perturbations in its diameter, will have sections, where it bulges out, and sections, where it pinches. Across a curved surface the Laplace pressure Δp will lead to pressure differences depending on the curvature of the surface given by [4, p. 8]

$$\Delta p = \gamma \left(\frac{1}{R_1} + \frac{1}{R_2} \right), \tag{1}$$

where γ is the surface tension, and R_1 and R_2 are the principal radii of curvature. Since the pinched regions of a liquid jet have a smaller circumference compared to bulged regions, their pressure will increase, which drives liquid flow towards the bulged regions. This will lead to further pinching and eventually to breakup, if the reduced wave number x of a sinusoidal mode in the jet radius along the propagation direction fulfills the condition [5]

$$x := \frac{2\pi}{\lambda} h_0 = \frac{2\pi f}{v_0} h_0 < 1. \tag{2}$$

Here, λ is the period length of the mode, h_0 is the undisturbed jet radius and ν_0 is the jet velocity. Further, the growth rate of such a sinusoidal mode depends on the Ohnesorge number $Oh = \nu \sqrt{1/\rho h_0 \gamma}$, where ρ is the density of the liquid and ν is its dynamic viscosity. For a given Ohnesorge number the relation between the growth rate of a sinusoidal mode in the radius of the jet and the reduced wave number can be estimated (see Fig. 1 c)).

This effect can be used to achieve controlled breakup of a liquid jet, by controlling the initial perturbations. To create the liquid jet, a capillary nozzle from Microjet Components [6] was used. It consists of a thin glass capillary, through which the liquid flows, and a piezo crystal, which is attached to the capillary's side and imprints perturbations on the jet (see Fig. 1 a)). When a voltage with a high frequency is applied, the crystal deforms periodically due to the piezoelectric effect, which leads to a vibration of the nozzle. Further, the piezo also applies pressure on the capillary depending on its deformation state. Hence, it disturbs the liquid pressure.

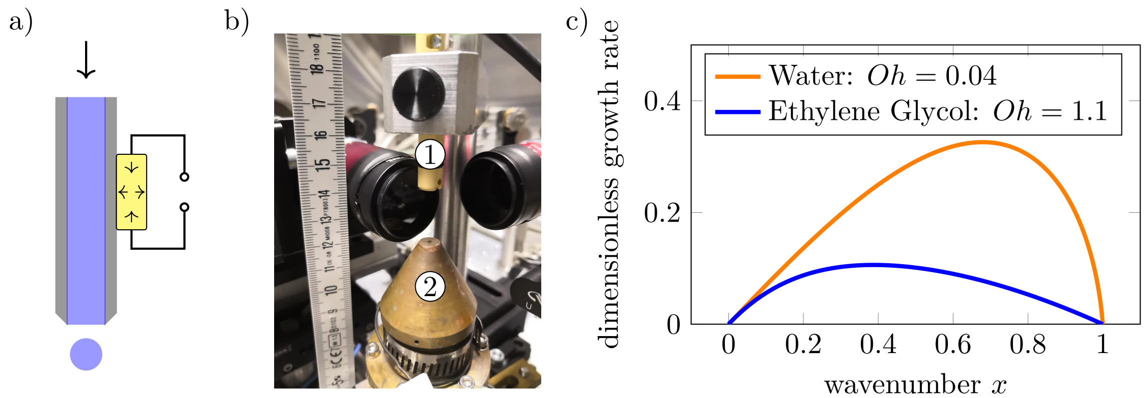

Figure 1. In a) a sketch of a capillary nozzle with an attached piezoelectric element is shown. Image b) shows a photo of the nozzle (1) and the droplet catcher (2) in a test chamber. In c) the relation between the growth rate of a sinusoidal mode in the radius of a jet depending on its reduced wave number is plotted for different liquids.

The nozzle used in the experiments has an exit diameter of 10 µm. As liquids, water (H_2O) with a vapour pressure of $p = 23$ mbar and ethylene glycol ($(CH_2OH)_2$) with a vapour pressure of $p = 0.08$ mbar [7] at 20 °C were used. The piezo was triggered using a HMF2550 frequency generator in burst-mode, which was triggered by the POLARIS laser's trigger system. The droplet source was positioned above a droplet catcher (see Fig. 1 b)), which was connected to a vacuum pump, so that the liquid affects the vacuum in the chamber as little as possible. The droplet catcher was heated to prevent the liquid from freezing.

In Fig. 2 the breakup process of a liquid water jet into droplets was observed via shadowgraphy. For the different images, the objective was moved a few mm along the vertical axis, to observe different parts of the breakup. In a) the nozzle can be identified as a shadow at the top of the image. The horizontal lines are due to light diffraction at the nozzle's edge. When the liquid jet leaves the nozzle, it has perturbations imprinted on it by the piezo crystal. The jet is periodically curved, which is probably due to the spatial vibrations of the whole nozzle with the driving frequency of the piezo crystal. Additionally, the thickness of the jet along its propagation varies slightly. When the bulge of the curvature is on the right side, the jet is thicker (cyan arrow). A probable reason for this is the change in the liquid pressure and the flow rate, induced by the piezo element. In b), c) and d) the perturbations in thickness grow in size due to the Laplace pressure (1). The sections where the jet is thicker, now bulge out to both sides. The size of these bulges increases until it is maximum in e) and f). There, the droplets have completely formed and are only connected by a thin thread. The ends of these threads pinch until they separate from the droplets in f) and g), which happens about 1 mm below the nozzle. The threads contract to reach the lowest possible energy state, and form so-called satellite droplets, which can be seen in g) and h). The upper and lower end of a thread do not separate simultaneously from the corresponding droplet. In Fig. 2 the threads stay connected longer to the upper droplet, which gives the threads an upward momentum. Therefore, the satellite droplets and main droplets merge again in j).

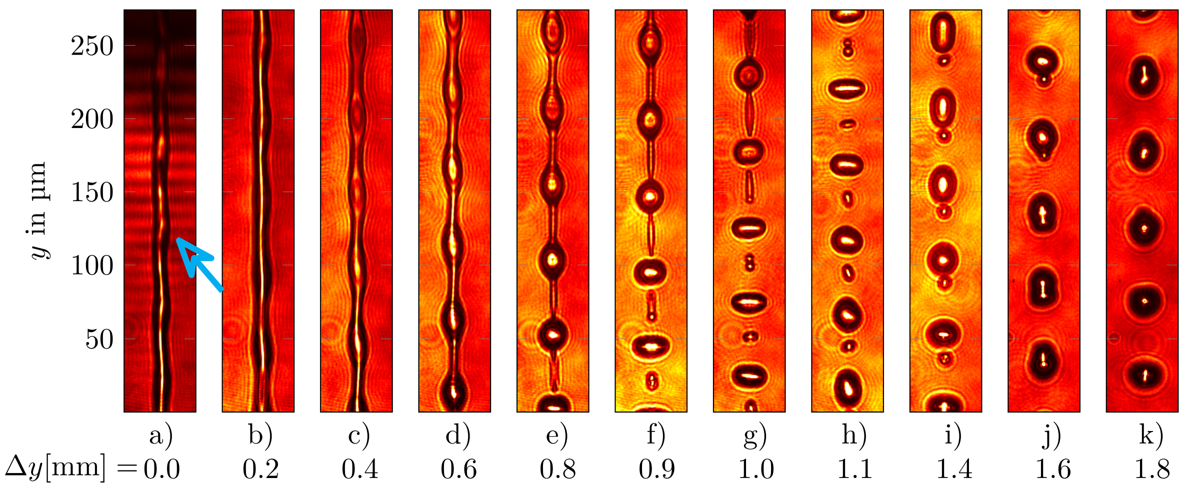

Figure 2. The images show a water jet, which was shot into vacuum with a pressure of 42 bar. On the piezo a frequency of $f = 1.39$ MHz was applied. Each picture from left to right is further away from the nozzle. Δy is the approximate distance from the top of the image to the nozzle.

Journal of Physics: Conference Series **3124** (2025) 012019 doi:10.1088/1742-6596/3124/1/012019

3. Droplet Stability

In our experiments, the FWHM of the laser's focus was significantly smaller than a droplet's diameter. To ensure accurate irradiation of a droplet, the droplets' positional stability was examined. For each set of jet and piezo parameters a series of probe pictures were taken, where the center of a fixed droplet was selected and its coordinates were saved. With these droplet positions the standard deviations in x- (horizontal) and y-direction (along the jet propagation) were calculated via

$$\sigma_x = \sqrt{\frac{1}{N}\sum_{i=1}^{N}(x_i-\mu_x)^2} \quad , \quad \sigma_y = \sqrt{\frac{1}{N}\sum_{i=1}^{N}(y_i-\mu_y)^2} \quad \text{and} \quad \sigma_r = \sqrt{\sigma_x^2+\sigma_y^2} \tag{3}$$

where N is the total number of pictures, and $\mu_{x/y}$ are the arithmetic means of the x and y positions. A series of shots consisted of 40-50 pictures, where a single image was taken every two seconds.

For water flowing through the capillary with a backing pressure of $p = 30\,\mathrm{bar}$ the most stable frequency was varying in a range from 1.2 MHz to 1.3 MHz on different days. With these parameters the reduced wavenumber was $x \approx 0.78$, which is in agreement with Fig. 1 c). The applied voltage to the piezo followed a sine-function, since using a square function or a saw tooth function produced less stable droplets. Instabilities in the y-direction were in most cases larger than those in the x-direction, because the variations in the x-direction are due to spatial vibrations of the nozzle and therefore strongly limited. The variations in the y-direction do not have the same limitation because they are caused by the breakup process.

In the same manner, different frequencies were tested for different pressures. As the pressure is increased, which increases the droplet velocity, the stream is stable at higher frequencies, since the reduced wave number should remain constant. Further, the stability got slightly better at a higher pressure. While at at $p = 30\,\mathrm{bar}$ the highest stability was achieved at $f = 1.2\,\mathrm{MHz}$ with $\sigma_x = 0.6\,\mu\mathrm{m}$, $\sigma_y = 1.1\,\mu\mathrm{m}$, and $\sigma_r = 1.2\,\mu\mathrm{m}$, the stability could be improved to $\sigma_x = 0.7\,\mu\mathrm{m}$, $\sigma_y = 0.5\,\mu\mathrm{m}$, and $\sigma_r = 0.9\,\mu\mathrm{m}$ at $p = 40\,\mathrm{bar}$ and $f = 1.45\,\mathrm{MHz}$. This can be explained by the fact that the droplets reach the interaction point in a shorter time. The reduced wave number in that case is also $x \approx 0.75$. Regardless of the stability, the pressure should always be above 30 bar, because otherwise the risk of water freezing at the nozzle would be too high.

The biggest improvement was made, after the nozzle's exit was moved $\approx 1.5\,\mathrm{cm}$ closer to the interaction point to a distance of $\approx 1\,\mathrm{cm}$ to the point, where the droplets were observed. After the breakup, the velocity and direction of each droplet varies slightly. Therefore, a larger propagation distance leads to higher shot-to-shot variations. The stability could thereby be improved to $\sigma_r = 0.7\,\mu\mathrm{m}$ at $p = 44\,\mathrm{bar}$ and $f = 1.35\,\mathrm{MHz}$, with $\sigma_x = 0.2\,\mu\mathrm{m}$ and $\sigma_y = 0.7\,\mu\mathrm{m}$.

Ethylene glycol differs from water in its higher dynamic viscosity of $\nu_\mathrm{ethylene} = 18.4\,\mathrm{mPa\,s}$ compared to $\nu_\mathrm{water} = 0.8\,\mathrm{mPa\,s}$ and its lower surface tension of $\gamma_\mathrm{ethylene} = 48.5\,\mathrm{mN\,m^{-1}}$ compared to $\gamma_\mathrm{water} = 72.8\,\mathrm{mN\,m^{-1}}$ at $T = 20\,°\mathrm{C}$ [8, p. 1122-1166], which results in an Ohnesorge number of $Oh_\mathrm{ethylene} = 1.1$ for ethylene glycol and $Oh_\mathrm{water} = 0.04$ for water. This will lead to a lower perturbation growth rate for ethylene glycol, and hence, to a lower droplet stability (see Fig. 1 c)). Due to the different viscosity, the jet velocity of ethylene glycol will be lower than the velocity of water at the same pressure ($v_\mathrm{water} = 70\,\mathrm{m\,s^{-1}}$ for water and $v_\mathrm{ethylene} = 23\,\mathrm{m\,s^{-1}}$ for ethylene glycol at $p = 50\,\mathrm{bar}$). Therefore, lower driving frequencies are required to achieve the same reduced wave number. The highest stability in ethylene glycol was found to be $\sigma_r = 0.9\,\mu\mathrm{m}$ at $p = 50\,\mathrm{bar}$ and $f = 0.407\,\mathrm{MHz}$, which is slightly worse than water. The variation in the x-direction was $\sigma_x = 0.3\,\mu\mathrm{m}$ and $\sigma_y = 0.9\,\mu\mathrm{m}$ in the y-direction. However, the frequency range over which the breakup was regular was significantly smaller for ethylene glycol. For $p = 30\,\mathrm{bar}$ the water droplets were stable from $f = 1.0\,\mathrm{MHz}$ to $f = 1.4\,\mathrm{MHz}$, while the breakup of ethylene glycol became random if the frequency deviated only 0.05 MHz. The highest stability was found for a wave number of $x = 0.55$. Fig. 1 predicts the highest growth for a perturbation at $x = 0.39$, but still a relatively high growth rate at $x = 0.55$.

4. Proton Acceleration with the POLARIS Laser System

To accelerate protons, intensities above $10^{19}\,\mathrm{W\,cm^{-2}}$ are necessary. Hence, in this chapter, the fully diode pumped, double CPA system POLARIS (Petawatt Optical Laser Amplifier for Radiation Intensive experimentS) was used, to irradiate the micro-droplet targets.

4.1. Experimental Setup

The schematic setup in the POLARIS target chamber is shown in Fig. 3. In the experiments, the POLARIS laser system produced pulses with a duration of $\approx 140\,\mathrm{fs}$ and energies of up to $\approx 10\,\mathrm{J}$ after the pulse compressor. A plasma mirror was used to improve the temporal intensity contrast (TIC) and to suppress pre-pulses [10]. The pulses were focused onto the droplet target by a 19° off-axis, 30 cm focal length parabola. The FWHM spot size was $A \approx 19\,\mathrm{\mu m^2}$ large, which contained a fraction of $q = 0.15$ of the total pulse energy. The droplets were created by the setup described in Sec. 2.

To observe the proton beam profile, a scintillator (BC-422Q by Saint Gobain) was used, which was positioned $\approx 32.2\,\mathrm{cm}$ away from the droplets' position. Its rear surface was imaged onto a gateable CCD. When a scintillator is hit by ionizing radiation, like electrons, protons, or

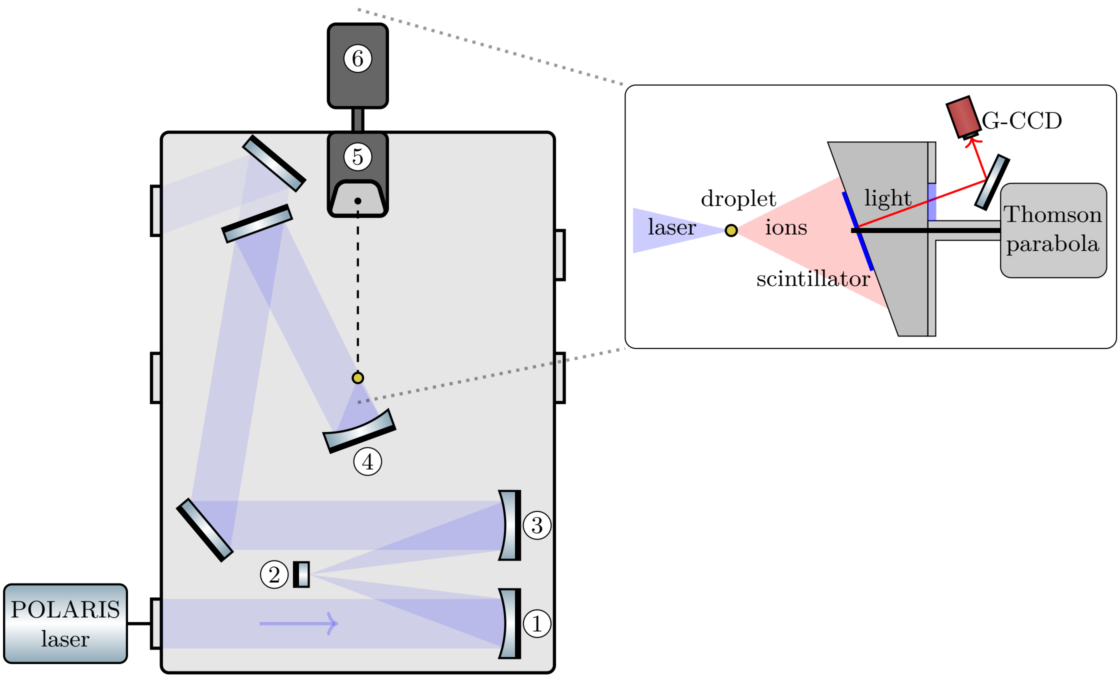

Figure 3. The image shows the experimental setup for the laser-plasma interaction in the POLARIS target chamber and the corresponding diagnostics [9]. An off-axis parabola (1) focuses the laser pulse onto the plasma mirror (2). A second parabola recollimates the beam (3). Finally, it is focused onto the target by a 19° off-axis, 30 cm focal length parabola (4). A scintillator (5) made the proton beam profile visible, which was observed with a gateable CCD-camera. A Thomson parabola spectrometer with a multi-channel plate (6) was used to measure the energy spectrum of the accelerated protons. The droplet source is indicated by the yellow dot. The figure is not to scale. A side view of the section from the droplet to the TP is shown in the box on the right.

ions, the irradiated spots emit light. To distinguish between the different particle species, their differences in time of flight between the target in the scintillator can be exploited by temporally gating the CCD camera. The scintillator was shielded from low-energy electrons, laser light and heavy ions by a 15 µm thick aluminum foil.

To examine the energy spectrum of the protons, a small tube lets a fraction of the accelerated protons pass through the scintillator, in the laser's forward direction, to a separate vacuum chamber containing a Thomson parabola spectrometer. A Thomson parabola (TP) [11] uses the superposition of an electric and magnetic field, which are aligned parallel to each other and perpendicular to the propagation direction of the ions. After the particles are separated by these fields, they hit a micro-channel plate (MCP-Detector S3810-25-I-PS by Scientific Instruments) with a phosphor screen, which can be imaged onto a CCD camera. From the positions where the ions hit the screen, single ion energies can be calculated, and the energy spectra can be reconstructed [12, Suppl.].

4.2. Proton Beam Profile

To effectively use the accelerated protons for applications, it is important not only to know their energies [12], but also to examine the spatial profile of the proton beam. This was done with the scintillator and a gateable CCD camera described in Sec. 4.1, which allows the simultaneous use of the Thomson parabola spectrometer.

The beam profiles from different shots and their respective proton spectra can be seen in Fig. 4 and Fig. 5. The shadow reaching from the bottom into the middle of the picture in Fig. 4 is due to the tube, through which protons can reach the TP. The bright spot right above that shadow, as well as the bright strip at the right edge of the picture, are due to leaking laser light. The images were taken as a part of a scan, which contained 95 shots for water and 97 shots for ethylene glycol. In all images, in which fast protons were detected, modulations were visible.

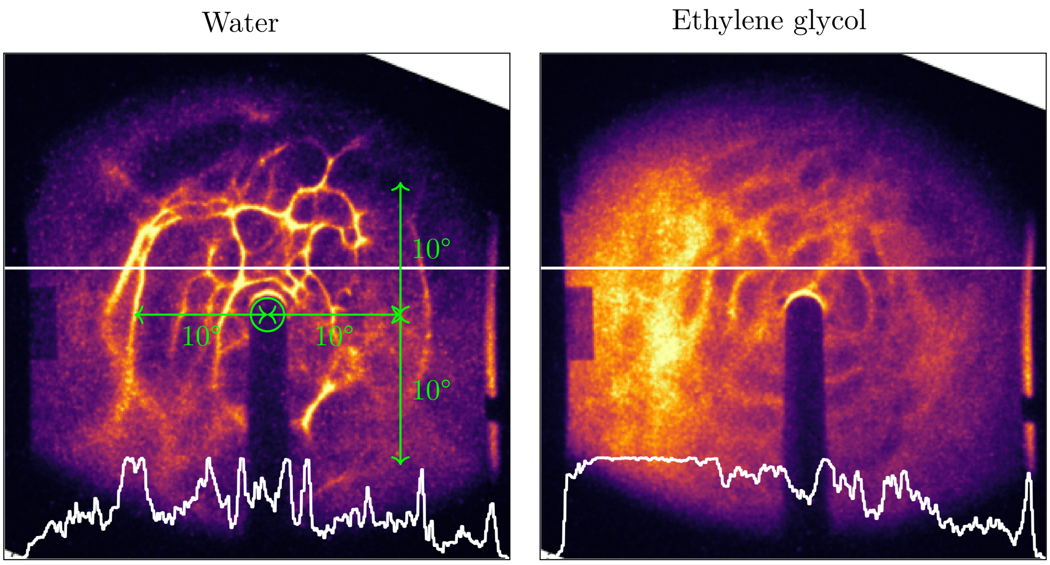

Figure 4. The proton beam profiles for different target materials are shown. The G-CCD camera was gated so that for water protons within an energy interval between 1 MeV and 7 MeV were observed. For ethylene glycol the observed proton energies ranged from 1 MeV to 6 MeV. The normalized brightness of the image at the white line is shown as a white graph at the bottom of each picture.

The modulations in the proton beam profile are more severe with water targets for comparable proton spectra (see Fig. 5). A possible explanation for this could be the mechanism proposed by L. Obst et al. [13]. There, the center of the laser focus is blocked by the mass limited target, which acts as a filter in the Fourier-plane. The laser light, which passes the droplet target, has higher spatial frequencies than the laser light, which is blocked by the droplet. This means that the electric field's distribution behind the target varies quickly in space. Since this field strength is high enough to ionize matter, the background gas will be ionized. While the electrons are displaced by the laser field, the ions of the background gas can be assumed to be stationary during the interaction, due to their higher mass. The corresponding electric fields, which can remain tens of picoseconds, are quasi static and only limited in time by the quasi neutral plasma expansion and energy loss due to electron-ion collisions. Therefore, they remain until protons accelerated by the TNSA-process pass through. The deflection of the protons by these fields likely leads to the modulations visible in Fig. 4. This may explain the more pronounced modulations when water droplets are used, because of the higher vapor pressure of water of 23 mbar compared to ethylene glycol with a vapor pressure of 0.08 mbar at 20 °C. Since more water will evaporate, more molecules will be present behind the water droplet and can be ionized by the laser light passing the droplet. This leads to stronger electric fields, and hence more pronounced modulations.

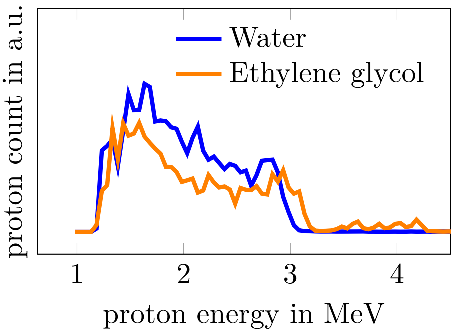

Figure 5. The energy spectra for the shots corresponding to the beam profiles in Fig. 4 are shown.

5. Conclusion

The generation of liquid micro-droplets from a jet was demonstrated for water and for ethylene glycol. This was done by connecting the nozzle to a piezo crystal, which was driven at a megahertz frequency. The resulting breakup of the liquid jet could be observed via shadowgraphy. The stability of the droplets was examined for different parameters, where water droplets were generally more stable than ethylene glycol droplets. To achieve the highest droplet stability for a given liquid, the reduced wave number must be chosen to maximize the growth rate of the external perturbations. Further, the nozzle should be moved close to the interaction point.

The micro-droplets were used as targets in proton acceleration experiments at the POLARIS laser system. There, density modulations in the proton beam profile could be observed, which were more pronounced for water compared to ethylene glycol. A likely reason for these modulations could be the interaction between the background gas and the laser's electric fields. The weaker modulations when using ethylene glycol could be explained by its lower vapor pressure.

6. Acknowledgments

This poster presentation has received support from the European Union's Horizon 2020 Research and Innovation programme under Grant Agreement No 101004730.

Journal of Physics: Conference Series **3124** (2025) 012019 doi:10.1088/1742-6596/3124/1/012019

References

[1] K. W. Ledingham, P. R. Bolton, N. Shikazono, and C.-M. C. Ma, "Towards laser driven hadron cancer radiotherapy: A review of progress," *Applied Sciences*, vol. 4, no. 3, pp. 402–443, 2014.

[2] J. Fernández *et al.*, "Fast ignition with laser-driven proton and ion beams," *Nuclear fusion*, vol. 54, no. 5, p. 054 006, 2014.

[3] P. McKenna *et al.*, "Lateral electron transport in high-intensity laser-irradiated foils diagnosed by ion emission," *Physical Review Letters*, vol. 98, no. 14, p. 145 001, 2007.

[4] J. Eggers and E. Villermaux, "Physics of liquid jets," *Reports on progress in physics*, vol. 71, no. 3, p. 036 601, 2008.

[5] L. M. Siqveland and S. M. Skjæveland, "Derivations of the young-laplace equation," *Capillarity*, vol. 4, no. 2, pp. 23–30, 2021.

[6] "Micro jet components - capillator - online shop." (), [Online]. Available: `http://www.microjetcomponents.com/2007CapillaryNozzle.htm`.

[7] C. for Diseasee Control, T. N. I. f. O. S. Prevention, and H. (NIOSH). "Pocket guide to chemical hazards." (), [Online]. Available: `https://www.cdc.gov/niosh/npg/npgd0272.html`.

[8] F. Cardarelli, *Materials Handbook*. Springer-Verlag London Limited, 2008.

[9] M. Beyer, *Development of Laser Sources and Diagnostics for Probing Relativistic Laser-Matter Interaction*. Master thesis. Friedrich-Schiller-Universität Jena, 2022.

[10] I. Tamer, "Petawatt-class laser optimization and ultrashort probe pulse generation for relativistic laser-plasma interactions," Ph.D. dissertation, 2020.

[11] C. Freeman *et al.*, "Calibration of a thomson parabola ion spectrometer and fujifilm imaging plate detectors for protons, deuterons, and alpha particles," *Review of Scientific Instruments*, vol. 82, no. 7, p. 073 301, 2011.

[12] G. A. Becker *et al.*, "Characterization of laser-driven proton acceleration from water microdroplets," *Scientific reports*, vol. 9, no. 1, pp. 1–8, 2019.

[13] L. Obst-Huebl *et al.*, "All-optical structuring of laser-driven proton beam profiles," *Nature communications*, vol. 9, no. 1, pp. 1–7, 2018.

The free version of DeepL (https://www.deepl.com/translator) was used to suggest english phrases.